

# Non-Uniqueness of the Geometry of Interplanetary Magnetic Flux Ropes Obtained from Model-Fitting

K. Marubashi<sup>1, 2</sup> and K.-S. Cho<sup>1,3</sup>

<sup>1</sup>Korea Astronomy and Space Science Institute, Daejeon, Republic of Korea

<sup>2</sup>Asia Space Environment Research Consortium, Chofu, Tokyo, Japan

<sup>3</sup>University of Science and Technology, Yuseong, Daejeon, Republic of Korea

E mail (kmaru\_bg@kzh.biglobe.ne.jp).

Accepted: 14 September 2015

**Abstract** Since the early recognition of the important role of interplanetary magnetic flux ropes (IPFRs) to carry the southward magnetic fields to the Earth, many attempts have been made to determine the structure of the IPFRs by model-fitting analyses to the interplanetary magnetic field variations. This paper describes the results of fitting analyses for three selected solar wind structures in the latter half of 2014. In the fitting analysis a special attention was paid to identification of all the possible models or geometries that can reproduce the observed magnetic field variation. As a result, three or four geometries have been found for each of the three cases. The non-uniqueness of the fitted results include (1) the different geometries naturally stemming from the difference in the models used for fitting, and (2) an unexpected result that either of magnetic field chirality, left-handed and right-handed, can reproduce the observation in some cases. Thus we conclude that the model-fitting cannot always give us a unique geometry of the observed magnetic flux rope. In addition, we have found that the magnetic field chirality of a flux rope cannot be uniquely inferred from the sense of field vector rotation observed in the plane normal to the Earth-Sun line; the sense of rotation changes depending on the direction of the flux rope axis. These findings exert an important impact on the studies aimed at the geometrical relationships between the flux ropes and the magnetic field structures in the solar corona where the flux ropes were produced, such studies being an important step toward predicting geomagnetic storms based on observations of solar eruption phenomena.

© 2015 BBSCS RN SWS. All rights reserved

**Keywords:** solar wind magnetic field, magnetic flux rope, magnetic field chirality, model-fitting

## 1. Introduction

We examined solar wind magnetic field structures during four periods which were selected as intervals of prominent solar terrestrial (ST) disturbances in the latter half of 2014 by the convener of the Space Weather Event Report Workshop. This workshop was held in March 2015 at Fukuoka, Japan, as a joint session with the 3<sup>rd</sup> Asia-Oceania Space Weather Alliance Workshop, and the United Nations Space Weather Workshop, 2015. The outline of the selected four ST disturbances had been distributed in advance by the workshop circular. In three cases out of the four, moderate geomagnetic storms are seen and the solar wind conditions exhibit the corresponding characteristic features. These three cases, Period A, Period B, and Period D as the convener named are the targets of this study. For the Period C, while the active region NOAA12192 produced many flares of M and X classes during its disk passage, no signature was clear that indicates the arrival of ICMEs near the Earth.

Since the early recognition of the importance of interplanetary magnetic flux ropes (IPFRs) as causes of geomagnetic storms (Zhang and Burlaga, 1988; Gonzalez *et al.*, 1998; Zhao and Hoeksema, 1998; Zhao, Hoeksema, and Marubashi, 2001), many attempts have been made to determine the structure of the IPFRs by model-fitting analyses to the observed magnetic fields in the solar wind as summarized in the next section. The first objective of this study is to confirm the existence of a flux rope structure in the solar wind

associated with each of the three periods (A, B and D) by finding out magnetic field variations that can be explained by flux rope model. In the model-fitting we tried to find out as many configurations as possible that can reproduce the observed magnetic field variations. As a result it has been found that each of the observed magnetic field structures can be reasonably well interpreted by three or four different configurations of flux rope models. Because such non-uniqueness of the IPFR geometries obtained by the fitting exerts a strong impact on studies aimed at the relationship between the IPFR structures and solar magnetic fields, it is the second objective to consider the conditions under which multiple geometries come out from the model-fitting. We present all the model results and discuss which is most reasonable when the solar source events are known.

## 2. Model-fitting analysis

The interplanetary magnetic flux rope has long been an active subject in the ST physics, since its discovery by Burlaga *et al.* (1981). One of the main concerns has been to determine its realistic geometry and magnetic field configuration. For this purpose many modeling techniques were developed. They include fitting to a cylindrically symmetric force-free model (Marubashi, 1986; 1997; Burlaga, 1988; Lepping, Jones, and Burlaga, 1990; Farrugia *et al.*, 1993), asymmetrically cylindrical non-force-free flux ropes (Mulligan and Russel, 2001; Hu and Sonnerup, 2002; Hidalgo *et al.*, 2002), and torus-shaped flux ropes

(Marubashi and Lepping, 2007; Hidalgo and Nieves-Chinchilla, 2012). Some comparisons among various fitting were performed by Al-Haddad *et al.* (2013) with the focus upon the performance of each fitting method. More recently, Wang *et al.* (2015) have developed a new model in which the poloidal motion in the flux rope is included. In this study we use both cylinder and torus models (Marubashi and Lepping, 2007) to determine the geometries of flux rope structures by the fitting method. The details of the toroidal field structure are described in the paper by Romashets and Vandas (2003). The flux rope parameters determined by the fitting are listed in Table 1 for the cylinder results and in Table 2 for the torus results.

We used the solar wind data from the Magnetic Field Experiment (MAG) and the Solar Wind Electron, Proton, and Alpha Monitor (SWEPAM) onboard the Advanced Composition Explorer (ACE). In addition, we also used the CME data from the Large Angle and Spectrometric Coronagraph (LASCO) onboard the Solar and Heliospheric Observatory (SOHO), and solar image data from the Helioseismic and Magnetic Imager (HMI) and the Atmospheric Imaging Assembly (AIA) onboard the Solar Dynamics Observatory (SDO), though the image data is not shown in the paper.

## 2.1 Period A

This period was selected with the intention to examine the cause of a moderate geomagnetic storm which gradually started around 03 UT on August 27, 2014. Figure 1 clearly shows that the IMF  $B_z$  were stably southward from 02 UT to 21 UT. At the bottom of Figure 1a we can see that the magnetic field variation is characterized by a smooth rotation in the Y-Z plane (in Geocentric Solar Ecliptic Coordinates). This field rotation is one of the typical characteristics of a magnetic flux rope. We performed a model-fitting analysis for the interval indicated by two vertical lines with a special attention to search all the possible geometries that reproduce the observed field variation in a reasonable way. As a result, three possible models were obtained: two cylindrical models and one toroidal model, all having negative (left-handed) chirality. Hereinafter, we call a magnetic flux rope with left-handed chirality an L-type flux rope, and one with right-handed chirality an R-type flux rope.

The modeled values are shown by red curves, Figures 1a and 1b for the cylinder models A-1 and A-2 in Table 1, and Figure 1c for the torus model A-1 in Table 2, respectively. The cylinder axis of model A-1 and that of model A-2 are completely different, the angle between the two axes being  $115^\circ$ . Nevertheless the calculated magnetic field values are similar to the observed values in both models. The prominent difference is seen in the  $B_x$  profile, that is, the earlier part is better reproduced by model A-1, whereas the latter part is better reproduced by model A-2. If we define a parameter,  $Erms$ , to evaluate the accuracy of fit by the root-mean-square of the difference between the modeled and observed values normalized by the

maximum observed value,  $Erms = 0.288$  (for cylinder model A-1),  $0.302$  (for cylinder model A-2) and  $0.331$  (for torus model A-1). While the torus model provides the worst fit of the three here, the overall feature of the calculated field variation is fairly similar to the observation, and it may well be that the fitted result is to be accepted. In addition, it is shown below that we could obtain a better torus fit by a special consideration

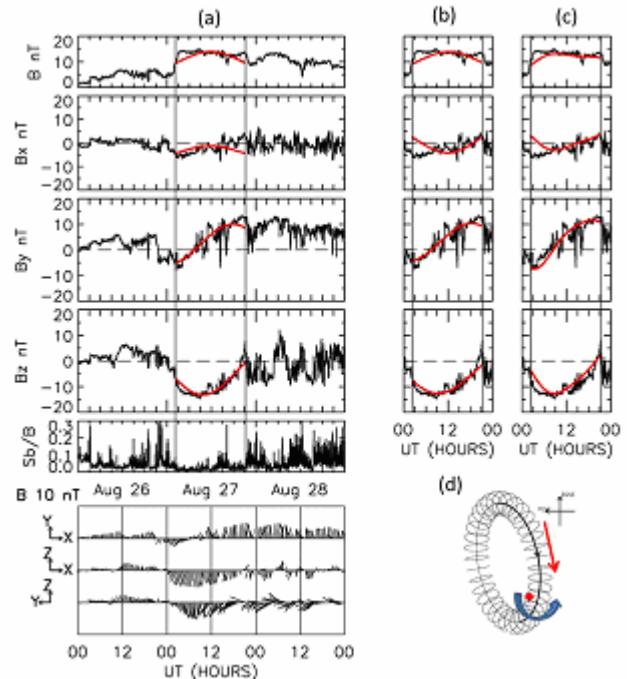


Figure 1: Comparison between the observed and modeled magnetic fields for the flux rope identified in Period A. (a) The result of fitting with L-type cylinder model (A-1) is shown in red curves. The plotted observed values are field intensity ( $B$ ), three components ( $B_x$ ,  $B_y$ , and  $B_z$ ), and fluctuations defined by the standard deviation divided by the intensity ( $S_b/B$ ). The bottom diagram shows field vectors projected on the X-Y, X-Z, and Y-Z plane. Note the smooth rotation of vectors in the flux rope in the Y-Z planes. (b) The result from another L-type cylinder (A-2). (c) The result from L-type torus (torus A-1). (d) A possible another torus model which is essentially equivalent to cylinder A-1.

It is straightforward, in this case, to find out the most likely solar source event for generation of the interplanetary flux rope. Therefore we can expect a possibility to determine what model is the most realistic by comparing the model geometry with the magnetic field structure in the solar source region. The transit time is estimated to be 132 hours by assuming constant speed of the flux rope (310 km/s, not shown in the figure). Then the launch time of the flux rope should be around 14 UT on August 22. The LASCO CME catalog ([http://cdaw.gsfc.nasa.gov/CME\\_list/](http://cdaw.gsfc.nasa.gov/CME_list/)) shows the occurrence of a halo CME which first appeared in the LASCO C-2 field of view at 11:12 UT on August 22. This is the only CME with width greater than  $120^\circ$  around this date. The CME was associated with a C2.2 flare peaked at 10:27 UT in the active region AR12146 at N12E01. The magnetic neutral line where the eruption

occurred was oriented  $255^\circ$ . Here the tilt angle,  $tilt_{NL}$ , is measured clockwise from the eastward (or Y-axis) direction from  $0^\circ$  to  $360^\circ$  by assuming the orientation of the sheared field matching the chirality of the corresponding interplanetary flux rope. In order to compare with this tilt angle, we estimated the tilt angle of the flux rope,  $tilt_{YZ}$ , defined by the orientation of the flux rope axis at the apex of the global loop configuration of the flux rope (Marubashi *et al.*, 2015). The results are:  $tilt_{YZ} = 295^\circ \pm 30^\circ$  (cylinder A-1),  $tilt_{YZ} = 296^\circ \pm 90^\circ$  (cylinder A-2), and  $tilt_{YZ} = 223^\circ$  (torus A-1). In addition we found another torus model, in which we removed the condition of the flank crossing for the torus fitting. One of the resultant geometries is depicted in Figure 1d. In this case we obtain  $tilt_{YZ} = 259^\circ$  as indicated by the red arrow, and  $Erms = 0.268$ . Thus we can say that the flux rope tilt angles in Figures 1a, 1b, and 1c are all roughly in agreement with  $tilt_{NL}$  of the corresponding solar magnetic field, while the model in Figure 1d gives the best agreement.

It is interesting to note the relationships between the cylinder and torus models. Firstly, the estimated range for cylinder A-2 looks too large as our attempt for determining flux rope geometry. The reason for this is that the cylinder axis direction is rather close to the X-axis. In such cases, generally, the cylinder models become less reliable and we should invoke the torus model. In fact, if we define the local axis orientation of the torus by the direction of a proxy cylinder around the place where the spacecraft crossed the structure, the local axis orientation of torus model A is given by latitude angle,  $\Theta_l = -14^\circ$ , and longitude angle,  $\Phi_l = 174^\circ$ . The orientation is close to that of cylinder A-2,  $\theta_\sigma = -23^\circ$ ,  $\phi_\sigma = 168^\circ$  (see Table 1). Secondly, the local axis orientation for the torus model in Figure 1d is estimated to be:  $\Theta_l = -46^\circ$  and  $\Phi_l = 21^\circ$ . They are very close to the corresponding values for cylinder A-1:  $\theta_\sigma = -42^\circ$ ,  $\phi_\sigma = 25^\circ$ .

## 2.2 Period B

This period was selected with main interest in the storm sudden commencement observed at 15:54 UT on 12 September at Kakioka, and the following moderate geomagnetic storm (minimum Dst = -75 nT at 0000 UT on 13 September). A large enhancement of solar energetic particles was also observed by GOES satellite, which started around 20 UT on 11 September and soon reached 30 pfu (proton flux unit). These observations suggested involvement of some energetic phenomena on the Sun in this period. Figure 2a presents the variations in the solar wind magnetic field for three day period from 12 September. The solar wind speed exceeded 600 km/s (not shown) after the passage of the shock indicated by the vertical dashed line. The magnetic fields are generally strong and stable in the interval shown by two solid lines, indicating that some kind of magnetic cloud passed the ACE spacecraft. It is clear that the geomagnetic storm was generated by the southward IMF in the sheath region just before the arrival of the magnetic cloud.

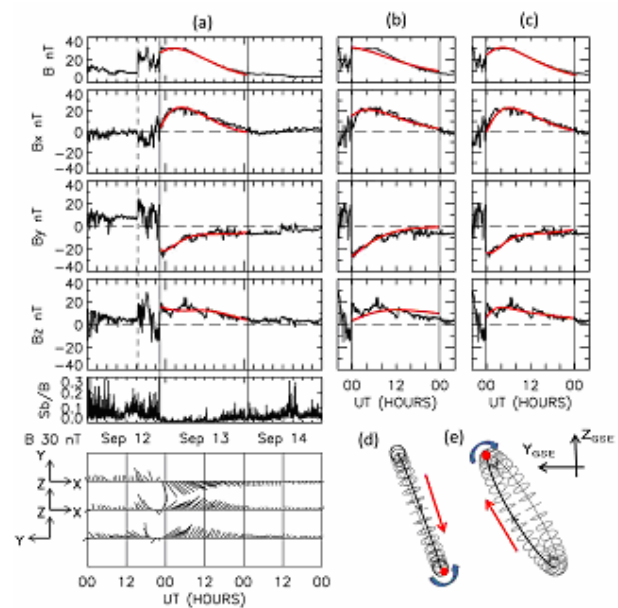


Figure 2. Comparison between the observed and modeled magnetic fields for the flux rope identified in Period B in the same format as that of Figure 1. (a) The result of fitting with L-type torus, (b) The result of fitting with L-type cylinder, and (c) The result of fitting with R-type torus. (d) and (e) depict the encounter of the spacecraft (red dot) with the L-type torus and R-type torus, respectively. The direction of  $tilt_{YZ}$  is also indicated by a red arrow.

While the field change is characterized by only small direction change as is evident in the vector plot at the bottom of Figure 2a, we executed fitting analysis to flux rope models. As a result we obtained three possible geometries of flux rope structure, the model profiles are plotted in red in the figure. Figure 2a shows the result of fitting with an L-type torus model ( $Erms = 0.127$ ), Figure 2b shows that of an L-type cylinder ( $Erms = 0.123$ ), and Figure 2c is for an R-type torus ( $Erms = 0.202$ ). Figure 2d and 2e show the geometries of the spacecraft encounter with the L-type and R-type torus models, respectively. It looks surprising that the modeled curves for the different chirality are almost identical. However, the similarity can be interpreted by considering the obtained fact that the spacecraft pass is nearly parallel to the local axis direction. The local axis direction for the case of the L-type torus is given by  $\Theta_l = 5.0^\circ$ , and  $\Phi_l = 3.5^\circ$ , whereas for the R-type torus  $\Theta_l = 1.6^\circ$  and  $\Phi_l = 349.6^\circ$ . Although the fitting to the cylinder model may look good at the first sight from the small value of  $Erms$ , closer looking reveals important discrepancy in the Bx value at the front boundary, and in the general trend in the Bz curve. Therefore, it should be said that the cylinder fitting is not satisfactory.

A halo CME occurred which first appeared in the LASCO/C-2 field of view at 18:00 UT on 10 September in association with the X1.6 flare at N14E02 in AR12158 peaked at 17:45 UT. It is of no doubt that this activity is related with the generation of the shock and the flux rope described above. However, the processes involved in this eruption are complex and the magnetic structure of the region is also complex.

Therefore we need more detailed analyses to identify the neutral line where the main eruption took place. The above flux rope analysis suggests some relevant eruption may have happened at the neutral line aligned more or less in the north-south direction where the magnetic polarity changes from positive on the east side to negative on the west side. At any rate, it is an important finding that the IMF variation can be reproduced by either of an R-type flux rope and an L-type flux rope.

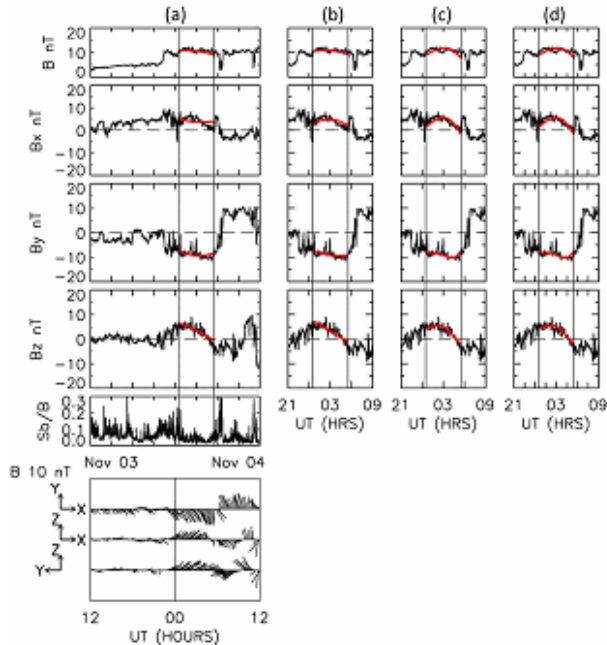


Figure 3. The results of fitting applied to the flux rope-like feature; with models of (a) L-type cylinder, (b) R-type cylinder, (c) L-type torus, and (d) R-type torus. Note that this IMF variation may not be attributed to a flux rope (see text).

### 2.3 Period D

This period was selected for detailed analysis aimed at possible space weather effects of a Hyder flare which occurred following a large filament eruption having occurred between 04 UT and 06 UT on 1 November centered around S20E40. Space weather phenomena listed in the WS circular include a weak geomagnetic storm with the minimum Dst of -38 nT on 4 November. The storm was apparently caused by the strong southward turning of IMF around 11 UT (not shown). However, it seems that the IMF change has nothing to do with the Hyder flare. In fact the associated CME expanded eastward and not toward the Earth. Several hours earlier than the storm, a noteworthy feature is seen in the solar wind magnetic field as shown in Figure 3, which exhibits a rotational variation like that of a flux rope during the interval indicated by two vertical lines. This may not be a flux rope but exhibit propagation of a torsional Alfvén wave (Marubashi, Cho, and Park, 2010; Gosling, Teh, and Eriksson, 2010), the correlation coefficient between the velocity and magnetic field being 0.73 (not shown). However, we performed the fitting analysis to the flux rope models, because magnetic

field variations associated with torsional Alfvén wave are generally similar to those of small-scale flux ropes grazed by spacecraft (Marubashi, Cho, and Park, 2010). Our basic idea is that similar field variations may be observed in the case of IPFR, and we tried to see what comes out from the flux-rope fitting in such cases.

As a result of the fitting analysis we obtained four possible geometries, which are compared with the observed variation in Figure 3: (a) the result from fitting by an L-type cylinder, (b) an R-type cylinder result, (c) an L-type torus, and (d) an R-type torus. The accuracy of fit is satisfactory for all of them (See Tables 1 and 2). It is safely supposed that the cylinder model yields a reasonable fit for both L- and R-type when the spacecraft crosses a flux rope at large distance from the cylinder axis (large impact parameter:  $|p| \cong 1$ ), because the observed magnetic fields are mainly constituted by the azimuthal component of the cylinder. The orientation of the cylinder axis for D-2 is close to the X-axis, the cone angle (angle between the cylinder axis and the X-axis) being  $15^\circ$ . Therefore the result for cylinder D-2 is less reliable as we discussed for cylinder A-2, whereas the local axis orientation of the torus D-2 is estimated to be:  $\theta_l = -7^\circ$ , and  $\Phi_l = 14^\circ$ , being very close to the axis orientation of cylinder D-2. Thus we can say that the result for torus D-2 is the more accurate version of the flux rope geometry corresponding to that for cylinder D-2. In the end, we conclude that three possible geometries were obtained for this structure.

### 3. Some consideration about the field vector rotation associated with a flux rope

It has long been accepted that the flux rope chirality can be uniquely inferred by the sense of field vector rotation observed in the Y-Z plane, since it was first pointed out by Marubashi (1986): Clockwise (anti-clockwise) field vector rotation corresponding to left-handed (right-handed) chirality. Bothmer and Schwenn (1998) extended the idea and presented classification about the field rotations into eight typical cases, which has been widely accepted. However, it should be noted that the above relationship between the flux rope chirality and the sense of field vector rotation does not always hold true when the cone angle of the flux rope axis is small and the spacecraft encounter the flux rope with large  $|p|$ .

Table 1. Results of the cylinder fitting for two flux ropes (A &amp; B) and for one flux rope-like structure.

Event ID	$r_0^a$ (AU)	$\theta_\alpha^b$ (°)	$\phi_\alpha^b$ (°)	$p^c$ ( $r_0$ )	$B_0^d$ (nT)	$U_0^e$ (km/s)	$T_0^f$ (hours)	$H^g$ L/R	$Erms^h$
A	<u>Start Time: 0215 UT on August 27, End Time: 2115 UT on August 27</u>								
A-1	0.068	-42	25	0.62	18.3	312	-4498	L	0.288
A-2	0.040	-23	168	-0.60	17.7	312	-726	L	0.302
B	<u>Start Time: 2215 UT on September 12, End Time: 0115 UT on September 14</u>								
B-1	0.115	-12	29	-0.96	59.5	631	36	L	0.202
D	<u>Start Time: 0030 UT on November 4, End Time: 0530 UT on November 4</u>								
D-1	0.033	12	206	-0.97	20.7	414	66	L	0.226
D-2	0.015	-6	14	0.93	20.1	413	89	R	0.197

## Legend

<sup>a</sup>  $r_0$  is the cylinder radius fitted to the flux rope at the time of encounter.

<sup>b</sup>  $\theta_\alpha$  and  $\phi_\alpha$  are the latitude and longitude angles of the field at the cylinder axis.

<sup>c</sup>  $p$  is the distance from the cylinder axis to the spacecraft.

<sup>d</sup>  $B_0$  is the magnetic field intensity at the cylinder axis at the time of encounter.

<sup>e</sup>  $U_0$  is the translational speed of the flux rope assumed constant.

<sup>f</sup>  $T_0$  is a parameter describing self-similar expansion of the flux rope.

<sup>g</sup>  $H$  indicates the handedness of the flux rope chirality (R: right-handed, L: left-handed).

<sup>h</sup>  $Erms$  is the root-mean square of the difference between observed and modeled values.

Table 2. Results of torus fitting\* for two flux ropes (A &amp; B) and one flux rope-like structure (D).

Event ID	$R_M^a$ & $r_m^a$ (AU)	$\theta_n^b$ & $\phi_n^b$ (°)	$sgnBx^c$ +/-	$p_y^d$ & $p_z^d$ ( $r_m$ )	$B_{T0}^e$ (nT)	$U_{T0}^f$ (km/s)	$D_T^g$ (km/s/h)	$T_0^h$ (hours)	$H$ R/L	$Erms^i$
A	<u>Start Time: 0215 UT on August 27, End Time: 2115 UT on August 27</u>									
A-1	0.203 0.0195	45 250	-	-0.64 -0.53	16.8	282	-2.9	-173	L	0.331
B	<u>Start Time: 2215 UT on September 12, End Time: 0115 UT on September 14</u>									
B-1	0.365 0.0563	23 271	+	-0.48 -0.31	58.6	685	4.6	32	L	0.127
B-2	0.389 0.0507	-29 79	+	0.40 0.13	52.9	690	5.0	31	R	0.123
D	<u>Start Time: 0030 UT on November 4, End Time: 0530 UT on November 4</u>									
D-1	0.083 0.0079	-37 264	+	-0.46 -0.62	18.0	414	0.1	149	L	0.175
D-2	0.112 0.0205	-67 120	+	0.10	22.5	411	-0.8	90	R	0.190

## Legend

<sup>a</sup>  $R_M$  is the major radius of torus, and  $r_m$  is the minor radius of the torus at the time of encounter.

<sup>b</sup>  $\theta_n$  and  $\phi_n$  are the latitude and longitude angles of a vector normal to the torus plane.

<sup>c</sup>  $sgnBx$  indicates the sign of  $Bx$  component of axial field on the side where the spacecraft encountered.

<sup>d</sup>  $(p_y, p_z)$  indicates the position of the spacecraft track from the torus axis in the Y-Z plane.

<sup>e</sup>  $B_{T0}$  is a parameter to determine the intensity of the toroidal magnetic field.

<sup>f</sup>  $U_{T0}$  is the translational speed of the torus at the time of encounter.

<sup>g</sup>  $D_T$  is the deceleration factor of the translational speed of the torus.

<sup>h</sup>  $T_0$  is a parameter describing the self-similar expansion of the flux rope.

<sup>i</sup>  $H$  indicates the handedness of the torus field (R: right-handed, L: left-handed).

<sup>j</sup>  $Erms$  indicates the accuracy of fitting, definition is the root-mean-square divided by maximum  $|B|$ .

\* For more details, refer to Marubashi and Lepping (2007).

Figure 4 shows two model field variations for a flux rope with the right-handed chirality directed  $\theta_a = 0^\circ$ ,  $\phi_a = 35^\circ$ , exemplifying that both clockwise and anti-clockwise rotations can be observed in the Y-Z plane. Because the axis is in the X-Y plane, the spacecraft observes  $B_z$  that comes from the azimuthal (in the cylindrical coordinates) component changing from northward to southward in this case. This  $B_z$  variations are the same for the spacecraft encounter for  $p = +0.6$  and  $p = -0.6$ . On the other hand, By component to be observed includes two contributions: one from the axial field and another from the azimuthal component. While the former is the same for the positive and negative impact parameters, positive in this case, the latter changes the sign in this case negative for  $p > 0$  and positive for  $p < 0$ , and its intensity increases as  $|p|$  increases. Thus, as  $p (>0)$  becomes large, the total  $B_y$  can be negative, and consequently the field vector rotation becomes clockwise. The above consideration explains a reason, at least partly, why both L-type and R-type models can be fitted to a single flux rope some times.

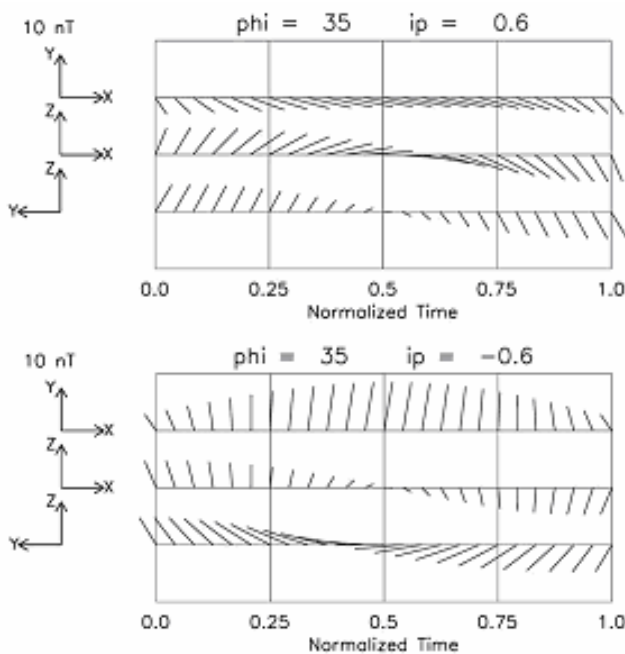


Figure 4. The magnetic field rotations to be observed by a spacecraft crossing a model flux rope of R-type with the axis orientation  $\theta_a = 0^\circ$ ,  $\phi_a = 35^\circ$ : (top) the encounter at  $p = 0.6$  exhibiting the clockwise rotation in the Y-Z plane, and (bottom) the encounter at  $p = -0.6$  exhibiting anti-clockwise rotation.

#### 4. Discussion

We have examined what geometries and models of flux ropes can reproduce the magnetic field variations observed by a spacecraft for three cases: two flux ropes, starting at 02:15 UT on 21 August and at 22:15 UT on 12 September 2014; and one flux-rope like variation starting at 00:30 UT on 4 November 2014. As a result, we have found three or four different geometries for each of the three cases that provide the modeled fields in reasonably good agreement with the observations. In particular, even the handedness of a flux rope cannot be determined by the fitting, that is, it has been seen that either of the R-type and the L-type models can reproduce the observed field variations in some cases. Such situations seem to occur for the spacecraft passage grazing the flux rope structure. Our simple model consideration has shown that the rotation of magnetic field vectors in the Y-Z plane observed by a spacecraft can be either clockwise or anti-clockwise depending on where the spacecraft encounters the flux rope. In conclusion, one important finding of this study is that the model fitting analysis does not always give us a unique solution for determination of the flux rope structure.

It has been an important issue to examine the relationships between the orientations of the flux rope axis and those of the neutral lines where the corresponding eruptions took place (e.g., Marubashi, 1997; Yurchyshyn, Wang, and Deng, 2001; Yurchyshyn *et al.*, 2007; Thernisien, Howard, and Vourlidas, 2006). The above conclusion has strong impact on such investigations. We need special attention in using the model fitting analysis to determine the geometry of interplanetary magnetic flux ropes. It is strongly recommended to further attempt to select the right geometry by invoking other available observations including three-dimensional observations like interplanetary scintillations and multi-spacecraft observations.

#### Acknowledgements

We thank the ACE/MAG and SWEPAM teams for the solar wind data, the SOHO/LASCO team for the CME data, and the SDO/HMI and AIA data for the solar data. We would like to acknowledge our thankfulness also to the ACE Science Center for distributing science data from ACE, and to the CDAW Data Center operated by NASA and The Catholic University of America in cooperation with the Naval Research Laboratory for maintaining the CME catalog.

This work was supported in part by JSPS Core-to-Core Program (B. Asia-Africa Science Platforms), Formation of Preliminary Center for Capacity Building for Space Weather Research and International Exchange Program of National Institute of Information and Communication Technology (NICT).

## References

- Al-Haddad, N., Nieves-Chinchilla, T., Savani, N.P., Möstl, C., Marubashi, K., Hidalgo, M.A., Rousev, I.I., Poedts, S., and Farrugia, C.J.: 2013, *Sol. Phys.*, **284**, 129. DOI: 10.1007/s11207-0130244-5.
- Bothmer, V. and Schwenn, R.: 1988, *Ann. Geophys.*, **16**, 1. DOI: 10.1007/BF00777872.
- Burlaga, L.F., Sittler, E., Mariani, F., and Schwenn, R.: 1981, *J. Geophys. Res.*, **86**, 6673. DOI: 10.1029/JA086iA08p066673.
- Burlaga, L.F.: 1988, *J. Geophys. Res.*, **93**, 7217. DOI: 10.1029/JA086iA08p066673.
- Farrugia, C.J., Burlaga, L.F., Osherovich, V.A., Richardson, I.G., Freeman, M.P., Lepping, R.P., and Lazarus, A.J.: 1993, *J. Geophys. Res.*, **98**, 7621. DOI: 10.1029/92JA02349.
- Gonzalez, W.D., Clua de Gonzalez, A.L., Dal Lago, A., Tsurutani, B.T., Arballo, J.K., Lakhina, G.K., Buti, B., Ho, C.M., and Wu, S.-T.: 1998, *Geophys. Res. Lett.*, **25**, 963. DOI: 10.1029/98GL00703.
- Gosting, J.T., Teh, W.-L., and Eriksson, S., *Astrophys. J. Lett.*: 2010, **719**, L36. DOI: 10.1088/2041-8205/719/1/L36.
- Hidalgo, M.A., Cid, C., Vinas, A.F., and Sequeiros, J.: 2002, *J. Geophys. Res.*, **107**, 1002. DOI: 10.1029/2001JA900100.
- Hidalgo, M.A. and Nieves-Chinchilla, T., *Astrophys. J.*: 2012, **748**, 109. DOI: 10.1088/0004-637X/748/2/109.
- Hu, Q. and Sonnerup, B.U.O.: 2002, *J. Geophys. Res.*, **107**, 1142. DOI: 10.1029/2001JA000293.
- Lepping, R.P., Jones, J.A., and Burlaga, L.F.: 1990, *J. Geophys. Res.*, **95**, 11957. DOI: 10.1029/JA095iA08p11957. DOI: 10.1016/0273-1177(86)90172-9.
- Marubashi, K.: 1986, *Adv. Space Res.*, **6(6)**, 335. DOI: 10.1016/0273-1177(86)90172-9.
- Marubashi, K.: 1997, in N. Crooker, J.A. Joselyn, and J. Feynman (eds.), *Coronal Mass Ejections, Geophys. Monogr. Ser.*, vol. 99, AGU, Washington, D.C., p. 147. DOI: 10.1029/GM099p0147.
- Marubashi, K. and Lepping, R.P.: 2007, *Ann. Geophys.*, **25**, 2453. DOI: 10.5194/angeo-25-2453-2007.
- Marubashi, K., Cho, K.-S., and Park, Y.-D.: 2010, in M. Maksimovic et al. (eds.), *12<sup>th</sup> Int. Solar Wind Conf., AIP Conf. Proc.* **216**, (Melville, NY: AIP), p. 240. DOI: 10.1063/1.3395845.
- Marubashi, K., Akiyama, S., Yashiro, S., Gopalswamy, N., Cho, K.-S., and Park, Y.-D.; 2015, *Sol. Phys.*, **290**, 1371. DOI: 10.1007/s11207-015-0681-4.
- Mulligan, T. and Russell, C.T.: 2001, *J. Geophys. Res.*, **106**, 10581. DOI: 10.1029/2000JA900170.
- Romashets, R.P. and M. Vandas, M.: 2003, *Geophys. Res. Lett.*, **30**, 1305. DOI: 10.1029/2003GL017692.
- Thernisien, A.F.R., Howard, R.A., and Vourlidas, A.: 2006, *Astrophys. J.*, **652**, 763. DOI: 10.1086/508254.
- Wang, Y., Zhou, Z., Shen, L., C. R., and Wang, S. J. : 2015, *Geophys. Res.*, **120**, 1543. DOI: 10.1002/2014JA020494.
- Yurchyshyn, V.B., Wang, H., and Deng, P.R.: 2001, *Astrophys. J.*, **563**, 381. DOI: 10.1086/323778.
- Yurchyshyn, V.B., Hu, Q., Lepping, R.P., Lynch, B.J., Krall, J.: 2007, *Adv. Space Res.*, **40**, 1821. DOI: 10.1016/j.asr.2007.01.059.
- Zhang, G. and Burlaga, L.F.: 1988, *J. Geophys. Res.*, **93**, 2511. DOI: 10.1029/JA093iA04p02511.
- Zhao, X.P. and Hoeksema, J.T.: 1998, *J. Geophys. Res.*, **103**, 2077. DOI: 10.1029/97JA03234.
- Zhao, X.P., Hoeksema, J.T., and Marubashi, K.: 2001, *J. Geophys. Res.*, **106**, 15643, DOI: 10.1029/2000JA000421.